# 6A.3 A STUDY ON THE EXTRATROPICAL TRANSITION OF TYPHOON XANGSANE (2000)

Cheng-Shang Lee* Kuo-chen Lu
*Department of Atmospheric Sciences, National Taiwan University*

## 1. Introduction

As a tropical cyclone moves poleward and interacts with the baroclinic environment, which includes the increased vertical wind shear and decreased sea surface temperature (SST), it evolves from an axisymmetric tropical cyclone to an extratropical storm (Jones et al. 2003). During the extratropical transition (ET), the temperature and wind fields of the cyclone become asymmetric with heavy precipitation often located to the north of cyclone track in northern hemisphere. Hart and Evans (2001) pointed out that 46% of tropical cyclones in the Atlantic basin underwent ET process. The ET often occurred at 45-50°N during the major hurricane season, but could occur as low as 30-35°N during the late season (October to November). In the western North Pacific, 27% of tropical cyclones that formed in June - October of 1994 -1998 transitioned to extratropical phase (Klein et al. 2000).

Taiwan located at 22-25°N often suffered from the heavy rainfall caused by a nearby typhoon when it moved poleward and interacted with the baroclinic environments in October and November, such as typhoons Zeb (1998), Babs (1998) and Xangsane (2000) in past 10 years. Among these systems, Xangsane is the most unforgettable one. When Xangsane skirted the east coast of Taiwan, a Singapore Airline airplane crashed while attempting to take off on a closed runway at Taipei International Airport killing 82 of the 179 passengers. On the other hand, a swath of heavy precipitation developed ahead of the storm center, extending from Taiwan to Okinawa, brought more than 1,000 mm rainfall to the island. Severe flooding and debris flows occurred around the whole island leading to 64 deaths. This paper attempts to study the extratropical transition of Xangsane, which occurred at latitudes as low as 25°N. In section 2, the synoptic environment of Xangsane during its ET phase is discussed. The MM5 model simulation of Xangsane and the comparisons against the observations are shown in section 3. In section 4, the structural changes and the related mechanisms are discussed. Finally, section5 is the summary and conclusions.

## 2. Observational analysis

Pre-Xangsane disturbance intensified to tropical storm intensity on 0600 UTC 26 October and to typhoon intensity on 0000 UTC 27 over the ocean east of Philippine (Fig. 1). During this period, Xangsane moved primarily west northwestward. After passing the Philippine islands, Xangsane changed its moving direction to toward the northeastward on 29 October. On 30 October, Xangsane reached its maxima intensity (about 90 kt) and began to speed up toward the north-northeast direction. From 31 October to 1 November, Xangsane, moving from the Bashi Channel along the east coast of Taiwan to Okinawa, increased its moving speed to above 20 kt – a common feature for tropical cyclone undergoing the extratropical transition process.

Observations showed that Xangsane maintained a well-defined typhoon structure on 1200UTC October 31 when it was located in the Bashi Channel. However, Xangsane lost its definition as a tropical cyclone 24 hours later when it was located in the East China Sea. Figure 2 shows the visible satellite imageries of Xangsane at 0400 UTC (1200LST) 31 October and 0400 UTC 1 November. When the center of Xangsane was located to the northwest of Luzon Island, deep convections still existed at the inner core region and around the system center (Fig 2a), although dense cloud also extended toward the northeast. In contrast, the deep convections were significantly suppressed on the southern side of the storm, at 0400 UTC 1 November when the storm center was located near the northeast coast of Taiwan. The open-cell cumuli were evident at the southwest quadrant, which clearly depicts the presence of the baroclinic zone.

At 0000 UTC 1 November, the surface and the 850 hPa analyses (Figs. 3a and 3c) revealed that strong cyclonic wind shear extends from the north of Taiwan to Japan, where dense cloud also presented. Significant cold advection was located to the north of the shear line and the warm advection, to the south, or a dipole pattern in temperature advection was located to the north of Xangsane. The surface high-pressure system (Fig. 3b) together with the cold air mass had moved southward to the central China. The 200-hPa upper level jet steak was just located to the north of Japan (Fig. 3b), with the entrance region of jet streak located at the East China Sea. Such upper level feature also favored the enhancement of the convection to the north Xangsane, or to the right hand side of the entrance region of the jet streak (Uccellini and Kocin 1987).

Besides the significant low-level temperature advection, the baroclinic zone was also associated with a significant vertical wind shear, by which the convection around tropical cyclone became asymmetric (Corbosiero and Molinari 2002, 2003). The intensity of Xangsane also weakened quickly, similar to that of a transitioning tropical cyclone (DeMaria 1996) as well. Figure 4 shows the vertical distributions of averaged zonal and meridional wind

* *Corresponding author address:* Cheng-Shang Lee, Department of Atmospheric Sciences, National Taiwan University, 1, Sec 4, Roosevelt Road, Taipei 106, Taiwan ROC; email: cslee@nat.as.ntu.edu.tw

speeds from 0000 UTC October 30 to 1200 UTC 1 November. Here the averaging was done for the area within 600 km from the storm center. Results showed that both zonal and meridional wind speeds increased significantly at upper levels after about 1200 UTC 31 October. The maximum wind speed occurred at 200 hPa. As Xangsane interacted with the baroclinic zone (or the upper level trough), the strong wind region extended downward to the mid-levels.

**3. MM5 Model Simulation**

To study the structural evolution and the associated mechanisms of Xangsane during the ET process, the NCAR/PSU MM5 was used to simulate the transition of Xangsane from a tropical cyclone to an extratropical storm. In this study, a triply nested domain was used as shown in Fig. 5, with grid spacing of 54 km, 18 km and 6 km, respectively. In the vertical, there were twenty three unevenly spaced full-sigma levels, with the maximum resolution in the boundary layer. One km terrain data of Taiwan were interpolated to the 6- and 18-km model grids using a Cressman analysis scheme. The Grell and Betts-Miller convective parameterization schemes were applied for 18- and 54-km domains, respectively. For the 6-km domain, the simple ice explicit moisture scheme was used. In the planetary boundary layer, the Blackdar scheme was used.

The initial time of the model simulation was 0000 UTC 30 October, when the center of Xangsane was located to the west of Luzon Island. Initial atmospheric conditions were generated by the interpolation of ECMWF (European Centre for Medium-Range Weather Forecasts) TOGA (Tropical Ocean and Global Atmosphere) Basic data (2.5 lat. x 2.5 long.) to the MM5 grid. However, the information that the TOGA Basic data could provide was too coarse to resolve the intensity and the center position of Xangsane. To improve the model simulation, it was necessary to bogus an initial vortex that was closer to the observed storm intensity. The initial vortex bogusing scheme developed by Jian et al. (2005) was used for the 18- and 54-km domains. The scheme requires to bogus a rankine vortex at 12 hours before the model initial time (or 1200 UTC 29 October). After 12 h integration, the model- generated vortex was relocated to the storm center position at 0000 UTC October 30 (or the model initial time). Results showed that such bogusing scheme could provide a more realistic initial vortex as shown in Fig 6. The bogus vortex significantly improved the inner core structure and the intensity. As shown in the figure, the radius of maximum wind decreased from 300 km to 150 km, and the bogus intensity was closer to the observation (90 kt, estimated by JTWC).

Results showed that the MM5 simulation could reproduce reasonably well the evolution of the synoptic pattern as well as the track and the intensity of Xangsane during the 60 h simulation. As shown in Fig 7, the model track is closed to the observation. Here the center position of model storm was determined as the center of the minimum sea surface pressure. In addition, the model also reproduced well the trend of the intensity change as shown in Fig. 8, although the intensity of the model vortex was slightly weaker. Because the model could simulate the synoptic environment well, the evolution of the vertical wind shear around storm center was also well simulated (Fig.9). As shown in Fig 9, the 200 hPa – 850 hPa vertical wind shear in the model increased from 7 $ms^{-1}$ at 0000 UTC 30 October to 24 $ms^{-1}$ at 1200 UTC 1 November, which was about the same as the ECMWF analysis.

**4. Analysis of Simulation Results**

Xangsane underwent ET process from 1200 UTC 31 October to 1200 UTC 1 November, as it passed the east coast of Taiwan and then headed toward Japan. According to the reports of the RSMC (Regional specialized Meteorological Center), the minimum sea surface pressure of Xangsane filled by 25 hPa within 24 hours, from 960 hPa at 0600 UTC 31 October to 985 hPa at 0600 UTC 1 November, which is about the same as that derived from the coarsest domain.

At 0600 UTC 31 October, the cross section of vertical structure along the moving direction across the center of Xangsane (Fig. 10) showed that Xangsane still maintained as a well-defined tropical cyclone at this moment. As shown in Fig 10, the maximum vorticity center was located at lower layers, with stronger vorticity extending to upper troposphere (or near 100 hPa). A warm core anomaly of about 7.3 K was located at 200 hPa, which is the classic vertical structure of a mature tropical cyclone as mentioned by Anthes (1982). Twenty-four hours later (0000 UTC 1 November), Xangsane was located at the East China Sea and was experiencing the ET process, with the intensity decreased to 988 hPa (comparable to the 985 hPa reported by RSMC). At this time, the vorticity maximum was located at the lower troposphere with the vorticity center tilted toward the down-shear side with height, along the moving direction of Xangsane. The magnitude of the upper level warm anomaly had reduced greatly and also shifted toward the down-shear side. At 500-600 hPa, the warm core was locates behind the maxima vorticity center (or on the up-shear side). A strong upward motion associated with convection at the down-shear side, and the downward motion at the up-shear side, showed the asymmetric structure at this stage of ET. Such down-shear tilt with height of the vorticity center observed during the ET of Xangsane is similar to that of hurricane Iris (Thorncroft and Jones 2000) and typhoon David (Klein et al. 2000).

Figure 11 shows the west to east cross section of equivalent potential temperature and wind field across the center of Xangsane at 0600 UTC 1 November to further highlight the asymmetric structure during the ET phase. The low equivalent potential temperature below 800 hPa to the west of Xangsane was resulted from the southward/cyclonic advection of the cold and dry air (Fig. 11). As compared to the stable region to the west of the storm

center, the east part of the storm had tropical characteristics, such as a convectively unstable mid-lower layer and an in-up-out secondary circulation pattern as observed in a typical tropical cyclone. This is likely the feature at stage 2 or 3 of ET process as discussed by Klein et al. (2000).

To illustrate the three-dimensional asymmetric structures of Xangsane at the ET stage, we performed a series of backward trajectory analyses for air parcels ending at the inner region of storm using 18-km grid simulation. Parcels located at 90 km to the south (numbered 1), east (2), north (3) and west (4) of storm center at 900, 700, 500 and 300 hPa were traced back from 0600 UTC 1 November for 5 hours (Fig 12). In the figure, trajectories were shown with respect to the moving storm center. Results showed that most air parcels enter the inner region of storm at 900 hPa come from the south, such as trajectories 1, 2 and 3 that have temperature and mixing ratio greater than 20°C and 16 g/kg, respectively. Air parcel 4, come from the north was colder and drier with temperature of 17.2°C and mixing ratio, 13.8 g/kg. This feature also illustrates the stable region at the lower levels to the west of storm (Fig. 5).

Results also showed that air parcels ending at the north of the storm center at 700, 500 and 300 hPa generally had increased its altitude for thousands of meters during past five hours (2502, 5111 and 3625 meters for 700, 500 and 300 hPa, respectively). In other words, air rose at the down-shear side and subsided at the up-shear side, which is in good agreement with the model reflectivity shown as shading in Fig 12. For example, air parcel 1 (ending at the south of storm center) at 500 hPa in Fig 12 subsided for 1054 meters (table 1), while it was passing the southwest quadrant of the storm. The temperature increased by 9.2°C (from -8.4°C to 0.8°C) and the relative humidity reduced by 28% (from 81% to 53%) during the 5 this period.

The trajectory analysis clearly showed the rising (sinking) of air parcels on the down-shear (up-shear) side, which increased significantly the horizontal temperature gradient of the storm. As the results, the vertical structure of tropical cyclone during the ET phase revealed that the warm core was located behind the vorticity center at lower levels. It is interesting to note that although Xangsane moved very fast at a speed of 35 kt, most air parcels still rotated around the storm center at middle levels.

To diagnose the mechanism of vertical velocity tendency, the vertical momentum budget was performed. Since MM5 is a non-hydrostatic model, the buoyancy and the pressure perturbation relative to a realistic three dimensional reference state (Zhang et al. 2000) were obtained using equations (1) and (2). The reference state of the virtual temperature was calculated first, then the reference pressure was calculated by integrating the hydrostatic equation using the reference state of virtual temperature The vertical momentum equation is shown in Equation (3), following Zhang et al. (2000) which analyzed the vertical acceleration in the eye wall of Hurricane Andrew (1992). The forcing terms for vertical acceleration shown on the right hand side of (3) are pressure gradient force (PGF), the local buoyancy force and the water loading (WL). The local buoyancy force is further decomposed into the thermal (BUTV) and the dynamic (BUP) buoyancy. The water loading (WL) includes $q_c$, $q_r$, $q_i$, $q_s$ which are the mixing ratio of cloud water, rainwater, cloud ice and snow respectively. The Coriolis force and the numerical diffusion are quite small and can be ignored when compare to the terms in (3).

$$p'(x,y,\sigma,t) = p(x,y,\sigma,t) - \overline{p}(x,y,\sigma,t) \quad (1)$$

$$T_v'(x,y,\sigma,t) = T_v(x,y,\sigma,t) - \overline{T_v}(x,y,\sigma,t) \quad (2)$$

$$\frac{Dw}{Dt} = -\frac{1}{\rho}\frac{\partial p'}{\partial z} + g\left(\frac{\overline{\rho}}{\rho}\frac{T_v'}{T_v} - \frac{p'}{p}\right) - g\left(q_c + q_r + q_i + q_s\right) \quad (3)$$

Since the storm had a tilted vertical structure at 54 h simulation (0600 UTC 1 November), the vertical momentum budget was performed for 51 h simulation (0300 UTC 1 November) using 18-km grid data. Results showed that a maximum vorticity center at the altitude of 1 km was located near the northeast coast of Taiwan at 51 hour. The cross section along the moving direction of Xangsane (about the direction of vertical wind shear) crossing the storm center showed that the maximum vorticity center was located at the lower levels (Fig. 13) with vorticity center tilted down-shear with height. A low center with 0.2 hPa perturbation pressure was located at the surface. Together with the maximum vorticity center, the low center also extended toward the down-shear side with height. A maximum perturbation pressure center with magnitude of 2.5 hPa was located at about 100 km to the down-shear side (or the northeast) of the surface low-pressure center. The magnitude of this perturbation pressure (2.5 hPa) is comparable to that (3 hPa) computed at the eyewall of hurricane Andrew (1992) (Zhang et al. 2000).

The vertical distribution of model reflectivity (Fig 14) showed that convections were located to the down-shear side of the storm center where the maximum perturbation pressure was located. Figure 14 also showed that at the convective region, the pressure gradient force (PGF) was positive. The maximum PGF (120 ms-1 h-1) was located at latitude of around 5 km where the buoyancy force and the water loading were negative. The summation of these three terms was still positive but the magnitude was less than 40 ms-1 h-1 which is of the same order as that of Zhang et al. (2000). On the up-shear side (or the clear region), the PGF was negative with maximum negative value (~ -60 ms-1 h-1) located right behind the low-level maximum vorticity center. The BU was positive (maximum amount of 40 ms-1 h-1) and was mainly contributed by BUTV.

In summary, the adjustment mechanisms among the vertical forcing effects for the down-shear side (convective region) and the up-shear side (the clear

region) are quiet different. At the convective region, the PGF is balanced mainly by BUP and WL. While at the up-shear side clear region the PGF is balanced mainly by the BUTV. However, the net effect of these forces is very small or about 20-40 ms-1 h-1 when compared to the gravity (~0.1% of gravity).

To illustrate the structural changes of Xangsane during the ET process, Fig. 15 shows the cross section of vorticity and perturbation pressure along the moving direction of the storm at 52 h to 54 h. During this period, distribution in the perturbation pressure on the down-shear side remained relatively unchanged (the value of the maximum perturbation pressure increased from 2.7 to 3.1 hPa). While at the up-shear side, a maximum perturbation pressure at altitude of 2-3 km, originally located behind the surface vorticity center at 51h, moved gradually toward the down-shear direction or closer to the surface vorticity maximum. The changes in the distribution of the perturbation pressure at the up-shear side might be important to the structural evolution during the ET process.

The existence of the meso-high in the mid-levels of the up-shear side would enhance the upward (downward) PGF above (below) the center of the meso-high. This effect then produced the thermal buoyancy term, which acted to resist the change of PGF. For example, the amount of low-level (~1.5 km height) PGF behind the surface vorticity center was about -100 $ms^{-1}h^{-1}$ at 54h (Fig. 16), or about twice as large as that associated with the near-surface meso-high on the down-shear side at 51h. The thermal buoyancy (BUTV) also increased due to the increase of the local virtual temperature. Such results indicated that the warming process also took place as the vertical structure became more tilted during the ET process. On the other hand, the temperature above the meso-high decreased associate with the upward PGF. These results are similar to the conceptual model of Klein et al. (2000) which was based on the satellite imagery and composite analysis. Results are also similar to the idealized simulation of Ritchie and Elsberry (2001).

## 5. Summary and Conclusions

This paper examined the extratropical transition (ET) of Typhoon Xangsane (2000) when it moved north northeastward along the east coast of Taiwan, from the Bashi Channel to the East China Sea on October 31 - November 1. The NCAR/PSU MM5 was used to simulate the structural changes of Xangsane during the ET process. Results showed that the model could simulate reasonably well the changes in synoptic and mesoscale circulation patterns, as well as the increase in the vertical wind shear. The track, intensity and cloud pattern of Xangsane were also well simulated. Analyses of observations and the model results showed that although Xangsane experienced the ET process at much lower latitudes, it had the common features of ET described by Klein et al. (2000). A down-shear tilt of the vorticity center occurred during the ET process. Analyzing the air parcel trajectories with respected to the moving typhoon center showed that the air parcels traveled cyclonically around the system center. The air rose on the down-shear side and subsided on the up-shear side leading to a warm core existed at the mid-lower levels behind the vorticity center.

Analyses also showed that when the vorticity center started to tilt toward the down-shear side, the maximum pressure perturbation (2.5 hPa) occurred near the surface and in front of the system (vorticity) center and the minimum pressure perturbation (0.2 hPa), at the vorticity center and near the surface. At the same time, a perturbation pressure maximum occurred at altitudes of about 2-4 km and behind the surface vorticity center. This perturbation pressure maximum, likely due to the forced subsidence, moved along the shear direction (closer to the system center) and to a higher altitude as the tilting of the center increased. The vertical momentum budget analysis depicted that this perturbation pressure maximum played a crucial role on the change of the thermal structure during the ET processes. The pressure gradient acceleration above the maximum perturbation pressure tended to enhance the upward motion and help the weakening of the upper level warm core. On the other hand, the downward pressure acceleration should have helped the building of the low-level warm core.


## Acknowledgement

The authors would like to thank Miss Erin Huang for her helps in manuscript preparation. The study was supported by the National Science Council of the Republic of China (Taiwan), No. NSC93-2625-Z-002-009 and No. NCS94-2111-M-002-019-AP1.


## References


Anthes, R. A., 1982: Tropical cyclones, their evolution, structure, and effects. Meteorological Monographs, Volume. 19, No. 41, *Amer. Meteor. Soc.*, Boston 208 pp.

Betts, A. K. and M. J. Miller, 1986: A new convective adjustment scheme. Part II: Single column test using GATE wave, BOMEX, ATEX and artic air-mass data set. *Quart. J. Roy. Meteor. Soc.*, **112**, 693-709.

Colle, A. B., 2003: Numerical Simulations of the Extratropical Transition of Floyd (1999): Structural Evolution and Responsible Mechanisms for the Heavy Rainfall over the Northeast United States. *Mon. Wea. Rev.*, **131**, 2905–2926.

Corbosiero, L. K. and J. Molinari, 2002: The Effects of Vertical Wind Shear on the Distribution of Convection in Tropical Cyclones. *Mon. Wea. Rev.*, **130**, 2110–2123.

——, and —— , 2003: The Relationship between Storm Motion, Vertical Wind Shear, and Convective Asymmetries in Tropical Cyclones. *J. Atmos. Sci.* **60**, 366–376.

DeMaria, M., 1996: The effect of vertical shear on tropical cyclone intensity change. *J. Atmos. Sci.*, **53**, 2076~2087.

Dudhia, J., 1993: A nonhydrostatic version of the Pen State/NCAR mesoscale model : Validation tests and simulation of an Atlantic cyclone and cold front. *Mon. Wea. Rev.*, **121**, 1493-1513.

Evans, J. L., and R. E. Hart, 2003: Objective indicators of the life cycle evolution of extratropical transition for Atlantic tropical cyclones. *Mon. Wea. Rev.*, **131**, 909-925.

Grell, G. A., J. Dudhia and D. R. Stauffer, 1994: A description of the fifth generation Penn State/NCAR mesoscale model (MM5). *NCAR Technical Note, NCAR/ TN-98+STR*, 121 pp.

Hanley, D., J. Molinari, and D. Keyser, 2001: A composite study of the interaction between tropical cyclones and upper-tropospheric troughs. *Mon. Wea. Rev.*, **129**, 2570–2584.

Harr, P. A., and R. L. Elsberry, 2000: Extratropical transition of tropical cyclones over the western North Pacific. Part I: Evolution of structural characteristics during the transition process. *Mon. Wea. Rev.*, **128**, 2613–2633.

Jian, G. J., Lee, C. S., and Chen, G.. T.-J., 2005: Numerical simulation of Typhoon Dot (1990) during TCM-90: The discontinuous track across Taiwan. *TAO* (in press)

Jones, S. C., and Coauthors, 2003: The Extratropical Transition of Tropical Cyclones: Forecast Challenges, Current Understanding, and Future Directions. *Wea. Forecasting*, **18**, 1052–1092.

JTWC, 2000: Annual tropical cyclone report. *Joint Typhoon Warning Center*, 399 pp.

Kimbal S. K., and J. L. Evans, 2002: Idealized numerical simulations of hurricane- trough interaction. . *Mon. Wea. Rev.*, **130**, 2210–2227.

Klein, P. M., P. A. Harr, and R. L. Elsberry, 2000: Extratropical transition of western North Pacific tropical cyclones: An overview and conceptual model of the transformation stage. *Wea. Forecasting*, **15**, 373–396.

Ritchie, E.A., and R.L. Elsberry, 2001: Simulations of the transformation stage of the extratropical transition of tropical cyclones. *Mon. Wea. Rev.*, **129**, 1462 – 1480.

Rotunno, R., and Klemp J. B., 1982: The influence of the shear-induced pressure gradient on thunderstorm motion. *Mon. Wea. Rev.*, **110**, 504–520.

Thorncroft, C. D., , and S. C. Jones, 2000: The extratropical transitions of Hurricanes Felix and Iris in 1995. *Mon. Wea. Rev.*, **128**, 947–972.

Uccellini, L. W., and P. J. Kocin, 1987: The interaction of jet streak circulations during heavy snow events along the east coast of the United States. *Wea. Forecasting.* **2**, 289-309.

Zhang, D.-L., Liu Y., and Yau M. K., 2000: A multiscale numerical study of Hurricane Andrew (1992). Part III: Dynamically induced vertical motion. *Mon. Wea. Rev.*, **128**, 3772–3788.

Table 1. The altitude (z), temperature (T), mixing ratio (q) and relative humidity (RH) along air parcel trajectory 1 ended at 500 hPa at 54 h as shown in Fig 12.

| Time | Z (m) | T (℃) | q (g/kg) | RH (%) |
|---|---|---|---|---|
| 49 | 6831 | -8.4 | 3.8 | 81 |
| 50 | 6452 | -5.9 | 4.1 | 76 |
| 51 | 5828 | 0.3 | 4.1 | 52 |
| 52 | 6139 | -3.2 | 4.4 | 69 |
| 53 | 6275 | -4.6 | 4.5 | 76 |
| 54 | 5777 | 0.8 | 4.4 | 53 |

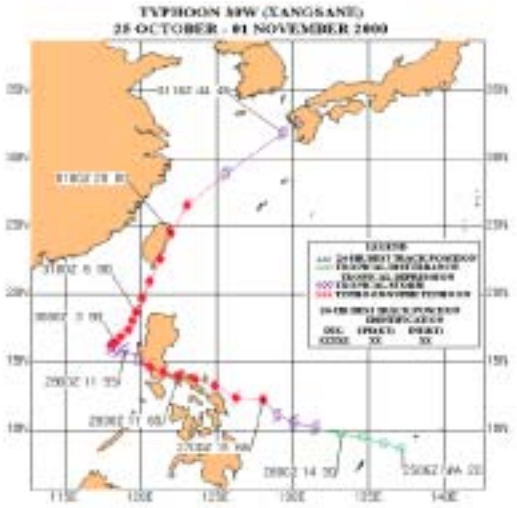


Fig. 1. The best track of Xangsane (2000). Symbols show 6-hourly positions (adapted from JTWC Annual Tropical Cyclone Report).

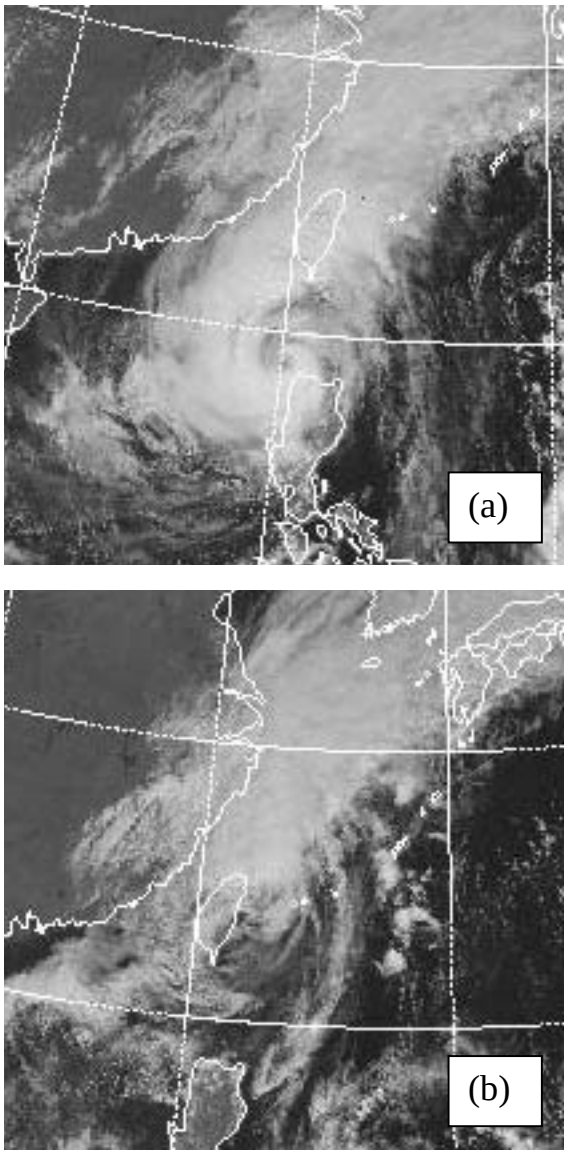


Fig. 2. GMS5 visible satellite image of Xangsane at (a) 0400 UTC (1200 LST) 31 October, and (b) 0400 UTC 1 November 2000.

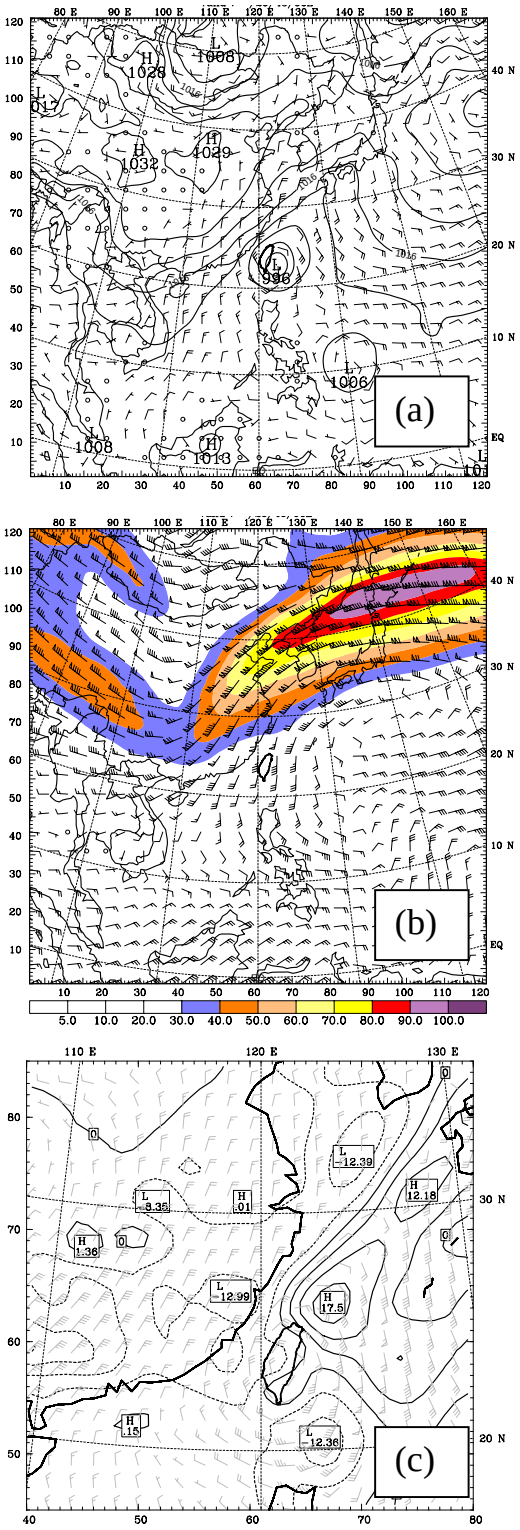


Fig. 3. (a) Sea surface pressure (every 4 hPa), and surface wind barbs (full barb = 10 kt), (b) 200 hPa wind barbs and total wind speed (shaded) and (c) 850hPa temperature advection (every 6 ℃ $s^{-1}$) at 0000 UTC 1 Nov. 2000.

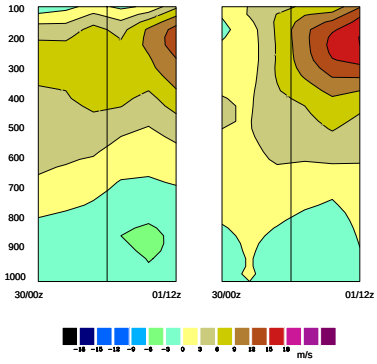


Fig. 4. Vertical distribution of zonal (left) and meridional (right) winds averaged within 600 km from the center of Xangsane from 0000 UTC 30 October to 1200 UTC 1 November 2000.

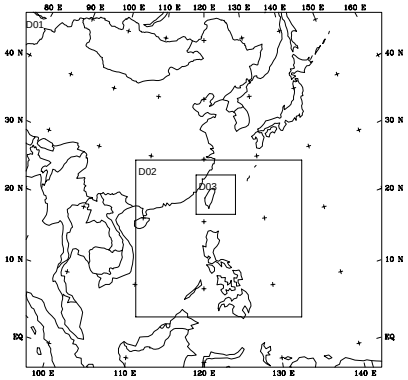


Fig. 5. Domains used for MM5 simulation.

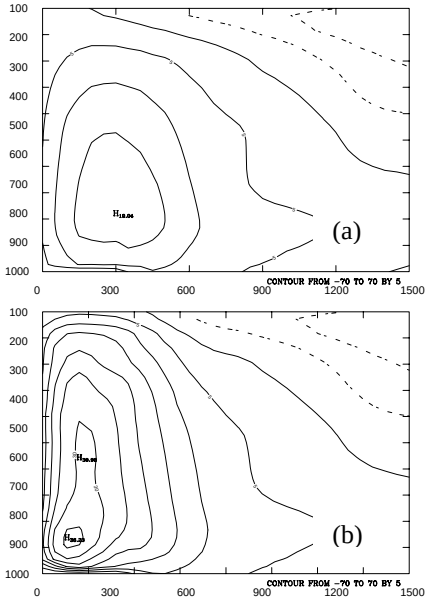


Fig. 6. Radial-height cross section of azimuthally averaged tangential wind for Xangsane at 0000 UTC 30 October. (a) ECMWF analysis, (b) after vortex bogusing.

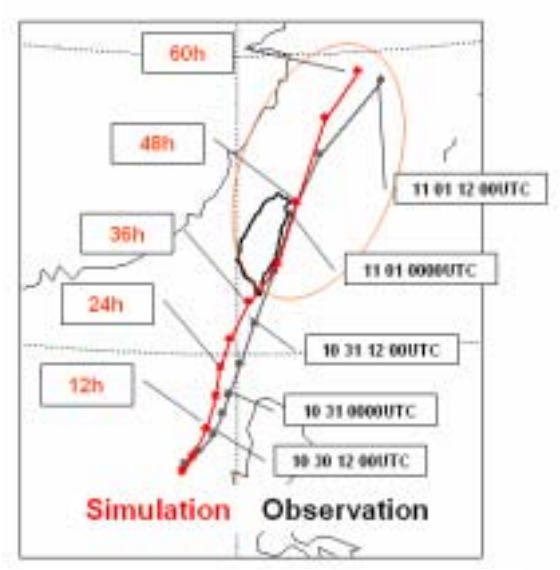


Fig. 7. Observed (labeled on the right side) and model simulated (labeled on the left side) tracks from 0000 UTC 30 October to 1200 UTC 1 November 2000.

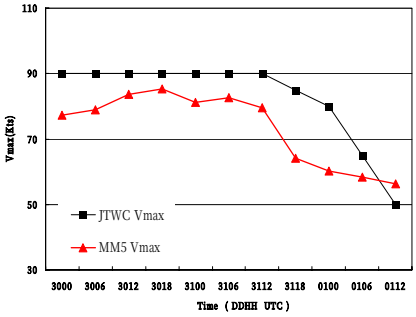


Fig. 8. Observed and Model-simulated intensity of Xangsane from 0000 UTC 30 October to 1200 UTC 1 November 2000.

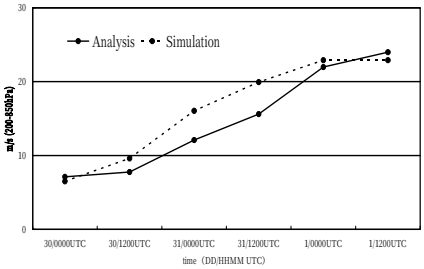


Fig. 9. observed (solid) and model-simulated (dashed) vertical wind shear ( 200 hPa – 850 hPa ) from 0000 UTC 30 October to 1200 UTC 1 November 2000.

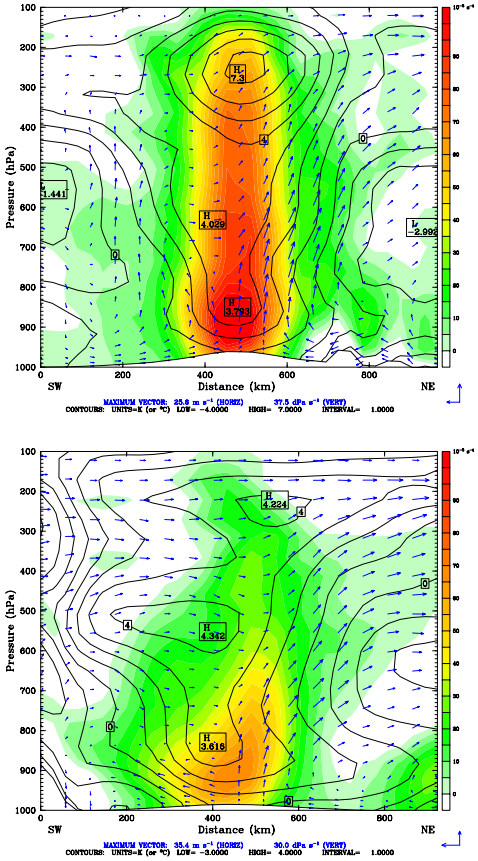


Fig. 10. Vertical cross section along the moving direction of Xangsane showing temperature anomaly (solid every 1 k), wind vectors along the moving direction and relative vorticity (shaded) for (a) 0600 UTC 31 October (30h), and (b) 0600 UTC 1 November 2000 (54h).

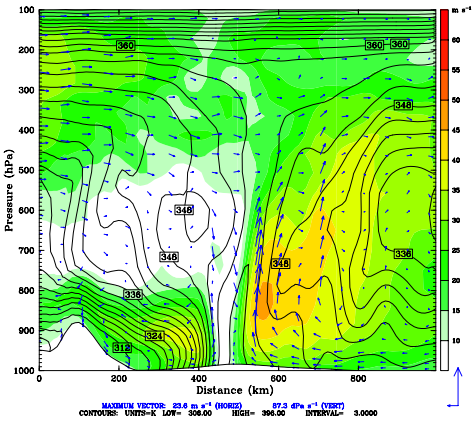


Fig. 11. West-east cross section along the center of Xangsane showing equivalent potential temperature (solid every 1 k), wind vectors along the cross-section and total wind speed (shaded, in $ms^{-1}$) at 0600 UTC 1 November 2000 (54h).

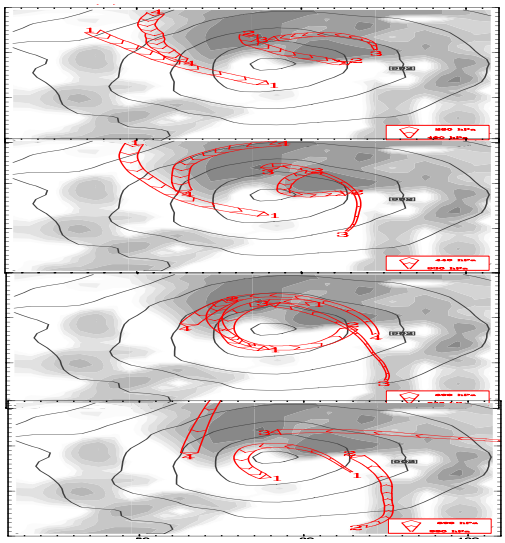

Fig. 12. Five-hour (49 h to 54 h) backward trajectories from 0600 UTC 1 November 2000 relative to the moving storm center for air parcels located at 90 km to the south (1),east (2), north (3) and west (4) of the storm center at 300 hPa 500 hPa 700 hPa and 900 hPa (from top to bottom)

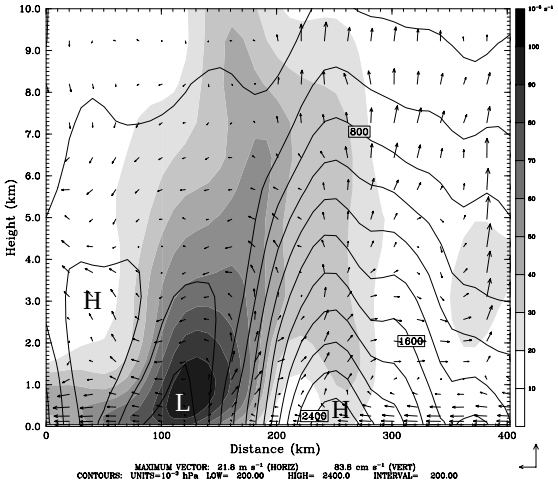


Fig. 13. vertical cross section along the moving direction of Xangsane, showing pressure perturbation (solid, every 200 mini hPa), wind vectors (relative to the moving storm) and relative vorticity (shaded $10^{-5}$ $s^{-1}$) for 51h simulation (0300 UTC 1 Nov. 2000).

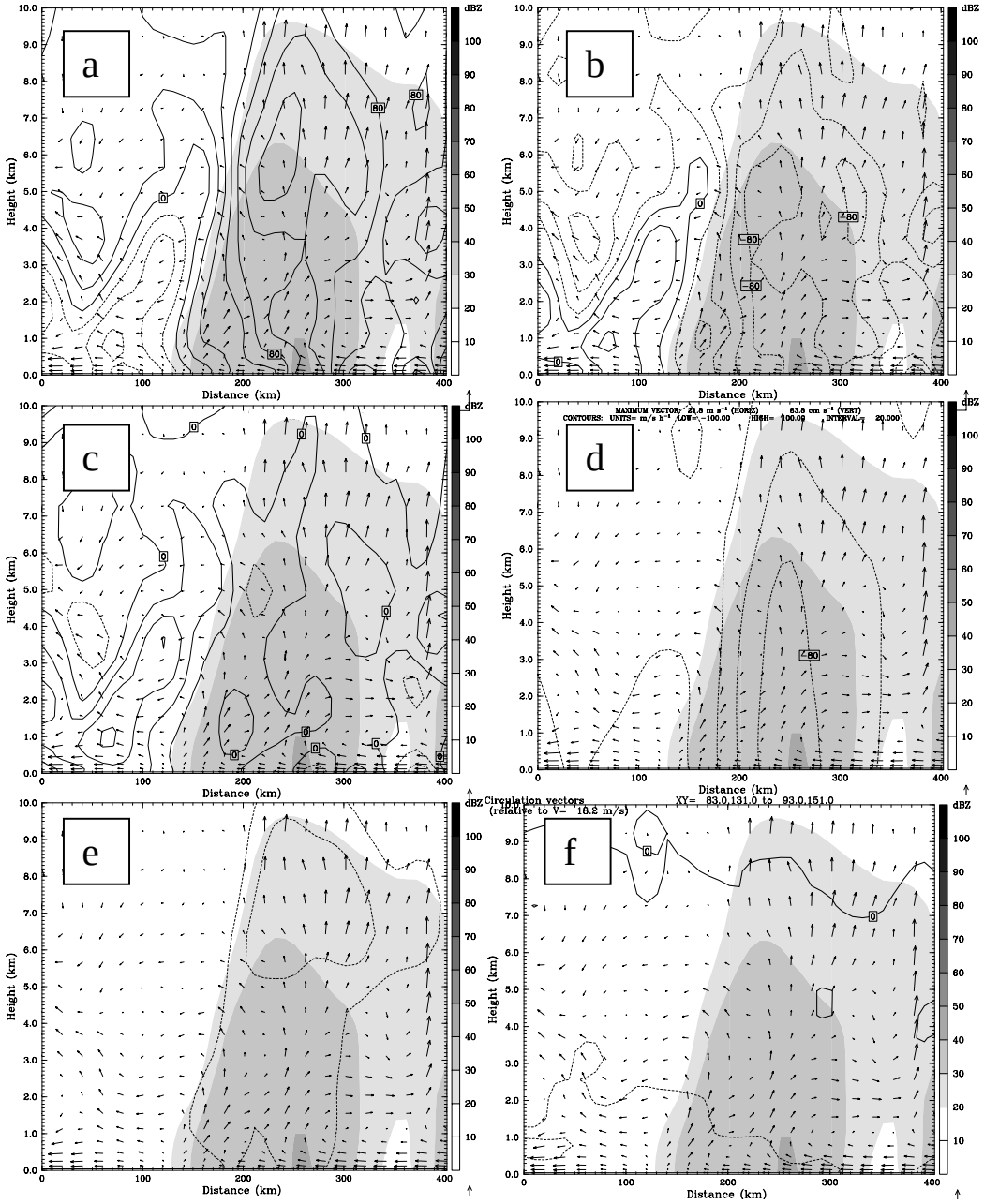


Fig. 14. As in Fig. 13 but for vertical momentum budget: (a) the perturbation PGF, (b) the buoyancy force (BU), (c) the thermal buoyancy force (BUTV), (d) the dynamic buoyancy force (BUD), (e) the water loading (WL), (f) summation (PGF + BU + WL). Dashed curves are negative values (every 20 $ms^{-1}h^{-1}$) The shading shows the reflectivity (in dBZ).

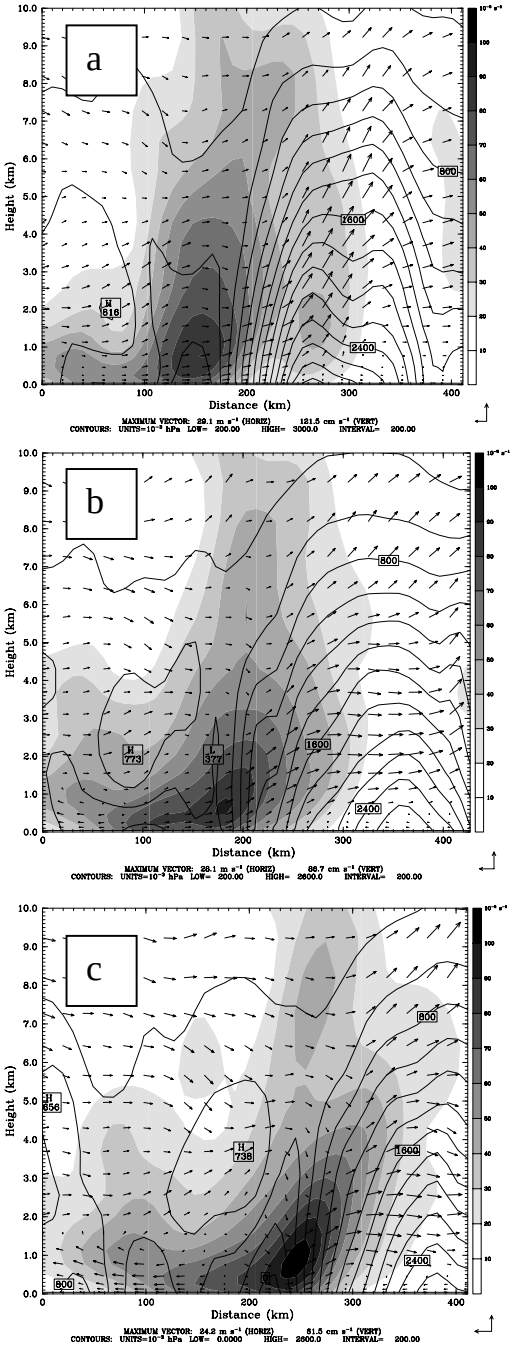


Fig. 15. As in Fig. 13, but for (a) 52 h, (b) 53 h and (c) 54 h simulation.

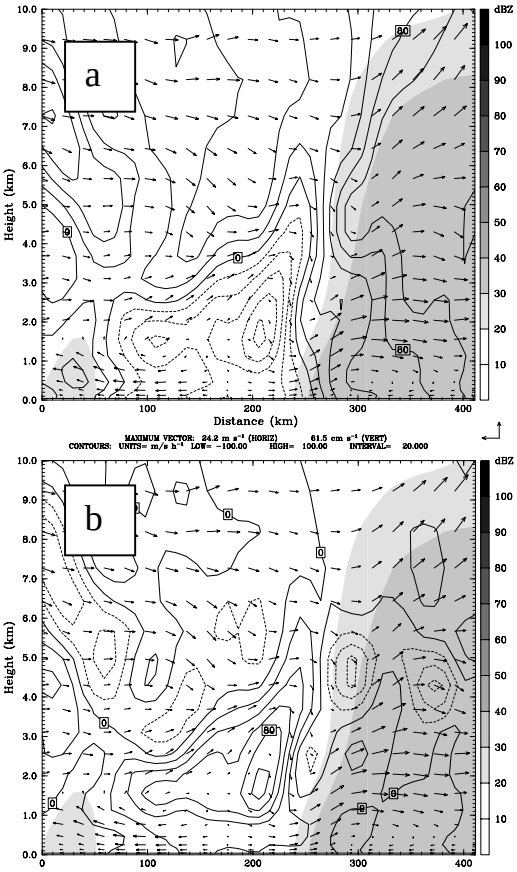


Fig. 16. As in Fig. 13, but for vertical momentum budget: (a) the perturbation PGF, (b) the thermal buoyancy force (BUTV).